Low-temperature Pd/FER NO_x adsorbers: operando FT-IR spectroscopy and performance analysis

Lidia Castoldi (Conceptualization)<ce:contributor-role>writing - original draft), Roberto Matarrese (Investigation) (Methodology), Sara Morandi (Investigation) (Writing - original draft), Pierfrancesco Ticali (Investigation), Luca Lietti (Supervision) (Writing - review and editing) (Funding acquisition)

PII: S0920-5861(20)30080-8

DOI: https://doi.org/10.1016/j.cattod.2020.02.019

Reference: CATTOD 12687

To appear in: *Catalysis Today*

Received Date: 27 October 2019

Revised Date: 25 January 2020

Accepted Date: 19 February 2020

Please cite this article as: Castoldi L, Matarrese R, Morandi S, Ticali P, Lietti L, Low-temperature Pd/FER NO_x adsorbers: operando FT-IR spectroscopy and performance analysis, *Catalysis Today* (2020), doi: https://doi.org/10.1016/j.cattod.2020.02.019

Low-temperature Pd/FER NO_x adsorbers: operando FT-IR spectroscopy and performance analysis

Lidia Castoldi[a], Roberto Matarrese[a], Sara Morandi[b], Pierfrancesco Ticali[b], Luca Lietti[a]*

[a] Department of Energy, Politecnico Di Milano, Milano, 20156, Italy

[b] Department of Chemistry and NIS, Inter-departmental Center, Università di Torino, 10125 Torino, Italy

*Corresponding author: luca.lietti@polimi.it

Graphical abstract

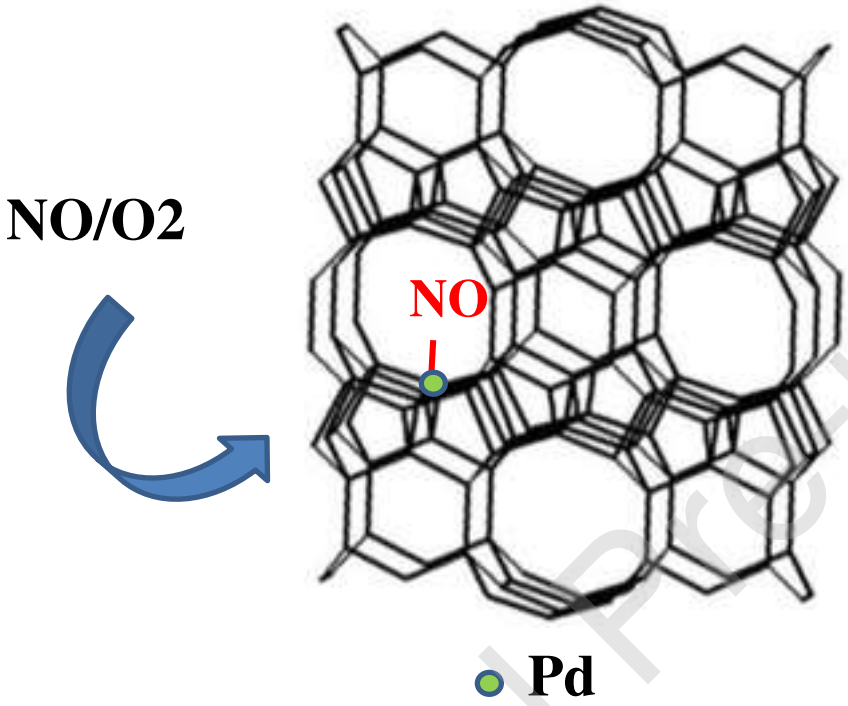

HIGHLIGHTS

- NO adsorbs as nitrosyls over Pd/FER
- NO displaces CO from Pd sites
- Pd/FER zeolite store NO at 80°C

Abstract

A Pd-doped FER zeolite sample is synthesized and investigated for potential use in the low-temperature NO_x adsorption. The catalyst is characterized by BET, XRD, TEM, NaCl titration and by *in-situ* FTIR spectroscopy following adsorption of CO, NH_3 and NO for the characterization of the Pd sites. Over the calcined sample, Pd is present mainly as PdO_x clusters/particles; near 13% of Pd is present in the form of isolated ions.

The NO_x adsorption / desorption performances at low temperature are investigated by microreactor studies and *operando* FTIR upon NO/O_2 adsorption followed by TPD under relevant operating conditions, i.e. in the presence of water and carbon dioxide. It is found that NO adsorbs in the form of Pd nitrosyls (hydrated and anhydrous) and nitrates; near 59 $\mu mol/g_{cat}$ of NO_x could be adsorbed, corresponding to a NO/Pd ratio near 0.6. Upon heating, nitrosyls decompose and transform into anhydrous species leading to NO desorption in the low-T region (below 200°C) and at higher temperature, with maximum near 370°C. The presence of CO negatively affects the NO_x storage capacity, due to a competition of CO and NO over the Pd storage sites.

Keywords: Pd-promoted zeolites, cold-start, Low Temperature NO_x adsorbers, PNA, Pd/ferrierite

1. Introduction

Mobile sources are nowadays responsible for a significant fraction of the total air pollution in urban areas. In case of diesel engines, major pollutants are carbon monoxide (CO), nitrogen oxides (NO_x) and particulate matter (PM); aftertreatment systems are adopted to reduce these pollutants and to meet the strict emission regulations. Typically, CO is controlled by a diesel oxidation catalyst (DOC), particulate matter by a diesel particulate filter (DPF), while NO_x are controlled by a selective catalytic reduction (SCR) or a NO_x-storage reduction (NSR) catalyst.

Concerning NO_x, SCR systems or NSR catalyst are effective after the correct operating temperature is attained. In the case of the SCR technology, the minimum operating temperature is related to the decomposition/hydrolysis of the injected urea to generate the active NH_3 reactant [1]. However, upon cold start the exhaust temperatures are relatively low and a period of 1 – 3 minutes is required for the diesel emission control system to become effective [2,3].

To address the cold-start problem, several approaches have been considered. A promising technique seems to be the use of the so-called passive NO_x adsorbers (PNAs) or low-T NO_x adsorbers (LTNAs): these systems store NO_x during cold start (i.e. below 200°C), and releases the stored NO_x once the deNO_x catalyst placed downstream has reached a suitable temperature [4,5].

In 2016 Johnson Matthey [6] reported a very efficient formulation for PNA systems based on acidic zeolites doped with Pd. In that work the authors compared different zeolite topology, like MFI, CHA, BEA, showing a marked NO_x storage capacity at 100°C and release at temperature suitable for that application, i.e. near 200°C. Research on zeolite-based LTNAs has intensified in recent years [6,7,8,9,10], since zeolites offers significant advantages in terms of hydrothermal stability and sulfur tolerance. Recently, Zheng et al. [8] have investigated several Pd-containing zeolites, and comparing different frameworks they concluded that the Pd-doped SSZ-13 zeolite seems to represent a very promising material.

In spite of the fact that several studies have already been published on this subject, still many aspects of the catalyst behavior (mechanism of adsorption; role of contaminants; nature of active sites, etc.) are not yet fully understood, as long as the role of the zeolite matrix. Accordingly, in this study a medium pore size zeolite (ferrierite) doped with Pd has been considered, and its NO_x trapping and desorption characteristics were evaluated under simulated exhaust conditions, i.e. in the presence of both H_2O and CO_2. Operando FT-IR spectroscopy and micro-reactor reactivity studies have been carried out trying to spread light on the relationship between catalyst performances and nature of adsorbed species.

2. Experimental

2.1. Catalysts preparation

The Pd-doped ferrierite used in this study (Pd_1/FER, Pd loading 1% w/w) has been prepared starting from a commercial zeolite (Zeolyst, Si/Al = 10), available in its NH_4-form. This support has been transformed into H-form by calcination at 700°C in air (1°C/min). Then the Pd_1/FER sample was prepared by impregnation of the zeolite support in excess of solvent using aqueous $Pd(NO_3)_2$ (solution at 4.5 % Pd, Sigma-Aldrich), followed by drying in air at 80°C overnight [11]. The dried precursor has been calcined with a two-ramp heating program, from room temperature up to 500°C (rate: 1°C/min, hold at 500°C 3 h) and then from 500°C up to 750°C (rate 5°C/min, hold at 750°C 2h).

2.2 Catalyst Characterization

BET analysis has been performed by adsorption-desorption of nitrogen at -196°C using a Micrometrics Tristar 300 instrument. Prior to the measurement all samples were degassed under vacuum at 350°C for 1 hour.

Information about the crystalline structure of the bare and Pd-doped zeolite was obtained from powder X-ray diffraction (XRD) using a Bruker D8 diffractometer with Cu Kα radiation. The XRD patterns were taken in the range of 10-50° (2 θ) with a step size of 0.05° at a speed of 12.5°/min.

Elemental compositions of FER and Pd/FER samples (both as such and Na-titrated) were analyzed by scanning electron microscopy (SEM) using a ZEISS EVO 50EP instrument equipped for energy-dispersive X-ray (EDX) spectroscopy (Oxford, INCA 200).

Morphological characterization of Pd_1/FER, oxidized at 500°C in 40 mbar of O_2, was performed by High Resolution Transmission Electron Microscopy (HR)-TEM using a side entry Jeol JEM 3010 (300 kV) microscope equipped with a LaB_6 filament. For the analysis the sample was deposited on a copper grid, coated with a porous carbon film. The digital micrographs were acquired by an Ultrascan 1000 camera and the images were processed by Gatan digital micrograph.

Quantification of the Brønsted acid sites and of isolated Pd sites has been achieved by NaCl titration [8]. This method selectively remove isolated Pd ions that are removed by Na^+, and hence allow the Pd speciation in terms of isolated vs. clusters or particles. Besides, the amounts of Na left on the sample may be used to quantify the concentration of acid sites. Briefly, in this method 50 mg of sample was stirred for 1 hour in a 0.1 M NaCl solution (50 ml) at 80°C. The solid has been separated by centrifugation and subjected again to the ion-exchange. Then, after a second centrifugation, the solid has been washed twice with distilled water, centrifuged and dried at 90°C.

The metal phase properties and the acidic character of the samples were determined by FT-IR spectroscopy upon adsorption of probe molecules (CO, NH_3, NO) in static conditions at RT. Absorption/transmission IR spectra were run at RT on a Perkin-Elmer FT-IR 2000 spectrophotometer equipped with a Hg-Cd-Te cryodetector, working in the range of wavenumbers 7200 - 1000 cm^{-1} at a resolution of 2 cm^{-1} (number of scans, ~ 60). For IR analysis, powder samples were pelletized in self-supporting disks (10-15 mg cm^{-2}) and placed in a quartz IR cell allowing thermal treatments in vacuo or in controlled atmosphere. Pellets were activated at 500°C by oxidizing or reducing treatment in O_2 (40 mbar) or H_2 (40 mbar), respectively. IR spectra were recorded at room temperature (RT) before and after interaction with CO, NH_3, NO and after subsequent evacuation at RT. In the figures, spectra are reported as difference spectra, where the subtrahend spectrum is that of the sample after the activation, before the gas admission.

2.3 Reactivity studies

Standard NO_x adsorption experiments were conducted both in a microreactor apparatus and in an *operando* FT-IT cell (#CSX, AABSPEC). In the first case, 60 mg of powdered catalysts, sieved at 70-100 µm, were loaded in a quartz microreactor with an internal diameter of 8 mm. The outlet of the reactor is directly connected to a mass spectrometer (ThermoStar 200, Pfeiffer Vacuum), a UV-analyzer specific for NO, NO_2, NH_3 (Limas 11HW, ABB), and a micro gas-chromatograph (3000A, Agilent). In a typical experiment, the sample was pre-treated under a flow of O_2 (3% v/v), CO_2 (2%

v/v), H_2O (2.5% v/v) (balance He) at a flow rate of 100 Ncm^3/min in the microreactor at 500°C for 30 min. Then the catalyst was cool down to 80°C and at this temperature, 300 ppm of NO are step-wise added to the gas mixture for 75 minutes. Then, NO supply is closed and the catalyst is heated under temperature programming (TPD) up to 500°C (heating rate 10°C/min).

The amounts of stored NO_x can be estimated from the area included between the reactor inlet and outlet NO_x concentration traces during the step input (adsorbed NO_x), or from the amounts of NO_x evolved during the TPD part of the experiment (desorbed NO_x). An inert tracer is present to check the goodness of the step changes in the concentration. The N balance, estimated from the difference between the adsorbed and desorbed NO_x, generally close within ± 5-10%.

In the case of the *operando* cell, the catalyst has been formed in self-supported wafers (7-12 mg cm^{-2}) and loaded in the IR cell reactor. The IR spectra (reported as difference spectra, using as background the spectrum obtained after the pre-treatment) were collected with a FT-IR Vertex 70 (Bruker, Billerica, MA, USA) spectrometer with 4 cm^{-1} spectral resolution. The outlet of the IR cell is connected to a FT-IR Multigas 2030 (MKS) for the gas analysis. The experimental procedure adopted in the *operando* cell was identical to that used for the microreactor rig but the space velocity was higher due to technical limitations in the minimum flow rate fed to the cell (25 Ncm^3/min).

3. Results and discussion

3.1. Catalyst characterization

3.1.1 Structural and Morphological Characterization

SEM/EDS analysis carried out over both the FER and Pd_1/FER samples confirm a Si/Al ratio near 10, and a Pd concentration near 1% w/w in the case of the Pd_1/FER sample.

Ferrierite is a medium-pore zeolite; its structure contains a 2D system of intersecting pores limited by 8- and 10-member rings (MRs) and is nonporous in the third direction [12]. The microstructure of the bare zeolite and Pd-doped catalyst forces to use a method to measure specific surface area more adequate than traditional BET equation. For this reason, according to literature indications [13] the

adsorption data were treated with the "t-plot" method developed by de Boer et al. [14], which is more suitable for solids containing micropores. FER exhibits a micropore area near 218 m^2/g, that is lower than the total surface areas calculated by the full BET equation, as expected. The addition of Pd does not modify the surface area, being 219 m^2/g the value calculated for Pd_1/FER.

XRD pattern obtained on the bare FER (Figure 1) is in agreement with the diffraction patterns for FER zeolite framework [15], shown for comparison purpose in the figure. The addition of Pd does not modify the zeolite structure, being the XRD spectrum of Pd_1/FER unchanged.

HR-TEM images of the Pd_1/FER sample are shown in Figure 2. Pd clusters or particles (darker particles) are present on several parts of the sample. These particles show dimensions ranging from a few nanometers up to 10 nm and they are constituted by an oxidized phases of Pd, as evidenced by FT-IR measurements (see below). As a matter of facts, NaCl titration used to quantify the amounts of isolated Pd ions [8] pointed out that the amount of exchangeable Pd is near 13%, in very good agreement with the data reported by Zheng [8] over Pd-doped Beta and SSZ-13 zeolites. It is suggested that the small amount of Pd exchangeable with Na^+ could be due to some small porosity in the zeolite that hinders the ion exchange between the Pd precursor and the zeolite. Accordingly significant amounts of Pd is likely located on external surfaces.

3.1.2 FT-IR Characterization

CO adsorption **-** To analyze the nature and accessibility of the Pd sites, the Pd_1/FER has been characterized by FT-IR spectroscopy upon adsorption of CO at r.t., and results are shown in Figure 3. The catalyst has been oxidized at 500°C in O_2 (40 mbar), cooled to r.t. and eventually CO has been added at increasing pressure up to 20 mbar. It is well evident the complexity of the spectra due to the presence of many carbonyl species related to Pd in different oxidation states and coordination. First of all, it is possible to divide the bands on the basis of the Pd oxidation state: in particular, bands in the regions 2220-2150 cm^{-1} and 2150-2110 cm^{-1} are assigned to carbonyls of Pd^{2+} and Pd^+,

respectively [16]. As a matter of fact, some authors ascribed the bands present at the higher wavenumbers (2214 and 2194 cm^{-1}) to carbonyls of Pd^{3+}/Pd^{4+} [8,17,18]. However, more recently, some of them disproved this assignment by combining experimental and density functional theory studies: they identified super electrophilic Pd^{2+} species, i.e. ion pairs with the negatively charged framework oxygens [19]. Finally, bands at 2060 and 1972 cm^{-1} are assigned to linear carbonyls of Pd^0 sites and to bridged carbonyls of Pd^+/Pd^0, respectively. The band at 1888 cm^{-1} was ascribed by some authors to multi-bridged carbonyls on small clusters such as Pd_3^0 or Pd_3O [8,20].

Inside the spectral region 2220-2150 cm^{-1} associated to Pd^{2+} carbonyls, it is possible to consider that the higher is the band frequency, the more is the site isolated. On this basis, we tentatively assign the bands at 2214-2194, 2173 and 2166 cm^{-1} to Pd^{2+} carbonyls present as isolated ions, small clusters or bigger particles, respectively. In particular, the couple of bands at 2214 and 2194 cm^{-1} are assigned to dicarbonyls of isolated Pd^{2+} ions, formed by ion exchange on the Brønsted acid sites and stabilized by the zeolite framework [19,21].

The assignment to isolated ions, small clusters or bigger particles of the bands at 2148, 2139 and 2119 cm^{-1} related to carbonyls of Pd^+ is not straightforward, being the Pd^+ carbonyls characterized by a significant π component of the Pd-CO bond. This accounts for a less separation of the bands, in particular of that at 2148 and 2139 cm^{-1}, which can be related to different aggregation states of Pd or to different framework position of isolated ions. Conversely, the band at 2119 cm^{-1} can be safely assigned to Pd^+ ions present as PdO clusters or particles [16 and references therein].

CO adsorption has also been performed after reduction at 500°C in H_2, and after re-oxidation at the same temperature. The corresponding FT-IR spectra are shown in Figure 4, traces b and c, respectively, where they are compared with the results of CO adsorption over the freshly calcined sample discussed above (trace a). For the reduced sample (trace b) it is well evident the absence of bands related to Pd carbonyls; the presence of a band at 2228 cm^{-1} can be assigned to carbonyls of extra-framework Al^{3+} [22]. The absence of bands related to Pd carbonyls suggests a marked coalescence of Pd during the reduction pre-treatment, forming big particles with very low amount of

exposed surface sites; indeed, the sintering of Pd under reducing conditions is well documented in literature [8,23]. The re-oxidation treatment (trace c) leads again to the appearance of the palladium carbonyl bands, indicating the Pd redispersion upon reoxidation of the reduced sample. However in the reoxidized sample (trace c) we note a marked increase of the Pd^{2+} components at the expense of the Pd^{+} ones with respect to the initial oxidation treatment (trace a). In particular, the bands related to dicarbonyls of isolated Pd^{2+} ions in the region 2220-2180 cm^{-1} are significantly increased, possibly indicating a higher dispersion of the PdO_x species upon reoxidation. This point will be further addressed below. Finally, the two bands in this high frequency region show the presence of shoulders, pointing out the heterogeneity of isolated Pd^{2+} sites.

Notably, re-oxidation after reduction does not lead back to the original oxidized state (compare traces *a* and *c*). However, the sample probed with CO after subsequent oxidation-reduction cycles showed that the catalyst behavior is reproducible, in that spectra similar to spectra *b* and *c* are obtained upon reduction-reoxidation, respectively.

NH_3 adsorption – Brønsted acid sites may play an important role in stabilizing Pd in a dispersed phase. For this reason, using NH_3 as probe molecule, we have investigated the Brønsted / Lewis acidity of the bare and of the Pd-doped zeolite, aiming at a better characterization of the extent of ion exchange of the Brønsted acid sites by Pd. Indeed, the adsorption of NH_3 at r.t. on a Brønsted site as ammonium and the ammonia adduct on a Lewis site is well discernable by infrared spectroscopy.

Figure 5 shows the spectra obtained after NH_3 interaction with oxidized FER and Pd_1/FER (section A), and of Pd_1/FER after oxidation, reduction and re-oxidation treatments (section B). The spectra were recorded after interaction with ammonia (2 mbar) and subsequent outgassing at RT, in order to eliminate weakly bonded NH_3. The band at 1463 cm^{-1} is assigned to the asymmetric bending of NH_4^+ ions formed by the interaction of ammonia with the Brønsted acid sites of the zeolite [24]. The integrated intensity of this band can be used for a rough estimation of the amount of Brønsted acid sites present on the bare FER. Indeed, according to the extinction coefficient for this vibration mode reported in the literature [25], a concentration of Brønsted acid sites near 0.3 mmol/g can be estimated. A similar

estimates (near 0.5 mmol/g) is obtained upon titration of the zeolite with NaCl. Notably, the theoretical acid site concentration, based on the Al content of the zeolite (and assuming an Al/acid site ratio equal to 1), is near 1.5 mmol/g. The discrepancy between the concentration of acid sites probed by NH_3 adsorption or by NaCl titration and the theoretical value is likely explained considering the presence of extra-framework Al^{3+}, as confirmed by CO adsorption experiments (see Figure 3).

The addition of Pd to the bare FER zeolite significantly decreases the amount of ammonium ions with respect to the bare zeolite (solid and dashed curves in Figure 5A, respectively), and this indicates that Pd^{n+} species give ionic exchange with Brønsted acid sites able to protonate ammonia. The Brønsted acid sites concentration after Pd addition is near the half of that estimated in the case of the bare FER sample.

The band at 1320 cm^{-1} in Figure 5A, solid line, is assigned to δ_{sym}(N-H) of NH_3 bonded to Pd^{n+} ions [26]. The corresponding δ_{asym}(N-H) mode is at about 1622 cm^{-1}, along with the δ_{asym}(N-H) mode of ammonia bonded to extra-framework Al^{3+} and the δ_{sym}(N-H) mode of NH_4^+.

Figure 5B shows the comparison of ammonia adsorption on Pd_1/FER after oxidation, reduction and re-oxidation at 500 °C. The spectra of the oxidized and re-oxidized sample (traces a and c, respectively) are very similar with bands at 1622, 1463 and 1320 cm^{-1} assigned as in Figure 5A. Moreover, they are very similar also taking into account the integrated area of the band at 1463 cm^{-1}: this means that the total amount of Brønsted acid sites exchanged with Pd^{n+} ions is almost the same after the first oxidation and following the re-oxidation treatments (compare trace *a* and *c* in Figure 5). At variance, the CO adsorption data previously shown revealed that the reduction-reoxidation cycle modifies the speciation of Pd^{n+} species, pointing out the formation of Pd^{2+} isolated ions at the expenses of Pd^+ moieties present non only as isolated ions (compare trace *a* and *c* in Figure 4), possibly pointing out the occurrence of a redispersion process. However ammonia adsorption does not put in evidence a significant change in the amount of Brønsted acid sites after oxidation and after re-oxidation, being the total integrated area of the 1463 cm^{-1} peak very similar in the two spectra.

This can be due to two contrasting factors, namely the increase of the clusters/particles PdO dimensions at the expense of Pd^{+} isolated ions on one side, and the concomitant to the increase of isolated Pd^{2+} species on the other side.

The spectrum obtained over the reduced sample (trace *b*) shows higher intensity of the band related to the δ_{sym}(N-H) of NH_4^+ ions at 1463 cm^{-1}: this means that on the reduced sample the amount of Brønsted acid sites is higher than that present on the oxidized one. This is in agreement with the results obtained upon CO adsorption that show a marked coalescence of Pd particles during the reduction: very likely, Pd aggregation leads to the restoration of Brønsted acid sites. Note that this reversibility in dispersion upon reduction−oxidation treatments is already reported in the literature for Pd/zeolites [8 and ref herein reported]. Moreover, for the reduced sample, the absence of the band related to the δ_{sym}(N-H) of NH_3 bonded to Pd^{n+} ions at 1320 cm^{-1}, present in the oxidized cases, confirms the reduction of Pd^{n+} to Pd^0.

In conclusion, Pd supported on the FER zeolite after oxidation comprises different forms, including mostly PdO clusters/particles and smaller amounts of Pd^{n+} isolated ions, as confirmed by NaCl titration, with Pd in different oxidation states like Pd^{1+}, Pd^{2+}. Reduction of the sample leads to Pd transformation into Pd^0 and agglomeration.

NO interaction - The nature of the species formed on Pd_1/FER oxidized at 500 °C after NO admission at r.t. at increasing pressure up to 2 mbar has been analyzed by FT-IR and results are displayed in Figure 6. Bands in the region 1900-1800 cm^{-1} are assigned to nitrosyl species of Pd^{n+}, although the oxidation state (Pd^{+} or Pd^{2+}) of the cation is still a matter of debate. Accordingly, the precise assignment of these bands is not straightforward [27]; moreover, both the positions of the nitrosyl bands and the absorption features are sensitive to the specific zeolite framework [6,28,29]. On these bases, bands at 1890 and 1873 cm^{-1} can be assigned to Pd^{2+} nitrosyls located in different zeolite positions (e.g. 10 or 8-ring channels) or present in different coordination states (isolated or in clusters/particles). At variance, the band at 1829 cm^{-1} can be assigned to Pd^{+} nitrosyls. In fact, according to the literature the NO stretching frequency of Pd^{2+}–NO nitrosyls is generally expected at

higher frequencies than those of the Pd^{+}–NO nitrosyls because of the lower π-back donation [18]. It is well evident that NO adsorption is not able to separate the contributions related to Pd^{n+} ions in different coordination states (isolated ions, clusters or particles) as in the case of CO adsorption.

Along with nitrosyl bands, peaks at 2167 and 1627 cm^{-1} are assigned to NO^{+} and adsorbed molecular water, respectively. These species are likely formed upon the reaction of NO with Brønsted acid sites in the presence of oxygen, as proposed by Hadjiivanov et al. [30]:

$$2\ NO + ½\ O_2 + 2\ O_{lattice}–H^{+} \rightarrow H_2O + 2\ O_{lattice}–NO^{+} \quad (1)$$

The pathway proposed in ref. 30 involves oxygen in the gas phase with the formation of gaseous NO_2. In our case oxygen is not present in the gas phase, but it is very likely present on the sample after the oxidation pre-treatment, in particular on the Pd phase. The involvement of adsorbed oxygen species for NO^{+} formation is clear by NO adsorption on the reduced sample, where no NO^{+} formation is evidenced in the IR spectrum (Figure 6B, b curve). Bands at 2250 and 1972 cm^{-1} are related to N_2O and NO_2 (adsorbed as NO_2^{+}) impurity in the gas, respectively [27]. On the reduced sample, un-reduced Pd^{2+} ions (band at 1873 cm^{-1}) are observed: reasonably, these are isolated ions stabilized by the zeolite framework.

3.2. Reactivity studies: NO/O_2 adsorption

The NO_x storage capacity of Pd_1/FER has been evaluated at 80°C feeding NO/O_2 mixture in the presence of CO_2 and H_2O. Note that two samples of Pd_1/FER have been considered, one calcined at 750°C and the other calcined at 500°C.

The profiles of NO adsorption and subsequent TPD are reported in Figure 7A-B in the case of catalyst calcined at 750°C and at 500°C, respectively. In both cases, upon addition of the NO/O_2 mixture, the NO concentration increases without dead time, reaching the inlet concentration value. The sample

calcined at 750°C shows a larger NO_x uptake if compared to the catalyst calcined at 500°C. Notably, no NO_2 is observed during the adsorption phase.

Considering the Pd_1/FER sample calcined at 750°C (Figure 7A), NO_x release occurs exclusively as NO during the thermal desorption (TPD) after the NO/O_2 storage. Two desorption peaks are visible, a low-temperature peak below 200°C and a high temperature peak above 300°C. More into details, the low-temperature peak presents two maxima at 100°C and 160°C, while the peak at higher temperature is centered near 370°C.

NO_x storage capacity has been estimated from the amount of NO_x desorbed during the TPD experiments; a value near 59 µmol/g_{cat} has been estimated, corresponding to a NO / Pd molar ratio of 0.6. This value suggests that not all the Pd is active in the NO storage under these conditions [6], in line with the presence of Pd species as cluster and/or big particles not active in the NO_x adsorption, as shown by the catalyst characterization. The storage capacity is anyway remarkable in spite less than 15% Pd is present as isolated moieties, as shown by NaCl titration.

In the case of Pd_1/FER calcined at 500°C (Figure 7B), the catalytic behavior is comparable under a qualitative point of view to that described in the case of the sample calcined at higher temperature (Figure 7A), but the amount of stored NO_x is much lower (21 vs. 59 µmol/g_{cat}). This clearly indicates that calcination at higher temperature increases the storage capacity of the Pd/FER, as already reported in the literature [31]. As a matter of fact, Ryou et al. found that hydrothermal treatment at high temperature up to 750°C induces transformation of bulk PdO into Pd^{2+}, thus favoring the low-temperature NO_x adsorption [31].

The NO/O_2 adsorption and subsequent TPD have also been studied by operando FT-IR spectroscopy. Being the performances of the high-temperature calcined system markedly better than those of the low-temperature calcined one, the operando FT-IR characterization was performed only on the system calcined at 750°C. The spectra obtained upon NO/O_2 adsorption in the presence of water and CO_2 are displayed in Figure 8. Several bands are observed in the 1870 - 1760 cm^{-1} region, at 1618 cm^{-1} and in the region 1500-1300 cm^{-1}. All these bands monotonically increase upon increasing the

time on stream. The bands in the 1870 - 1760 cm^{-1} region are related to Pd^{n+} nitrosyls; in particular it is possible to hypothesize that the bands at 1866 and 1844 cm^{-1} are related to Pd^{2+} and Pd^{+} nitrosyls, respectively, while bands at 1812 and 1762 cm^{-1} to the corresponding hydrated Pd^{n+} nitrosyls complexes. In fact, according to the literature, the coordination of a water molecule to Pd^{n+}-NO complex is expected to decrease the NO stretching by ca. 50 cm^{-1} [18,27,32,33]. The bands of anhydrous nitrosyls at 1866 and 1844 cm^{-1} are red-shifted of 7 cm^{-1} and blue-shifted of 15 cm^{-1}, respectively, with respect to the corresponding nitrosyl bands found in anhydrous conditions as shown in Figure 6A. The small differences in positions can be related to a slight modification of the overall Pd^{n+} electronic properties due to the presence of both CO_2 and water.

The band at 1618 cm^{-1} is related to the bending mode of adsorbed molecular water; this band is already present before feeding NO and it continuously grows upon the NO storage. Being water present in the feed stream, this indicates the progressive hydration of the surface at 80°C.

Finally, broad bands also apparent in the region 1500-1300 cm^{-1}. In particular the bands at 1437 cm^{-1} and 1335 cm^{-1} can be likely associated to $\nu_{asym.}(NO_2)$ and $\nu_{sym.}(NO_2)$ modes of monodentate nitrates [11].

Of note, the spectra show the absence of coordinated NO^{+} with bands near 2150-2106 cm^{-1}, that on the other hand has been observed under dry conditions (see Figure 6). This likely indicates its displacement by water at the Brønsted acid sites [6].

The obtained data provide further details on the adsorption pathways involved in the NO_x storage over Pd-doped zeolites. It is well known that the adsorption of NO_x is influenced by the zeolite framework, the Pd dispersion and the feed composition (mainly the presence of water and/or reductants) [6,8,34,35]. However, it is recognized that highly dispersed Pd cations are involved in the storage of NO_x; these species are favored at low Pd loadings whereas at high Pd loadings PdO clusters may also be formed [8]. Brønsted acid sites and the zeolitic framework structure are known to play important roles in determining the states of Pd, including dispersion, distribution, and oxidation states, as well as local structures. In particular, in the presence of water (as in our experiments) formation of

neutral $Pd^{(II)}(OH)_2(H_2O)_2$ complexes upon hydrolysis of zeolitic Pd cations is expected, as suggested by Epling et al. [35]. Hydrated Pd-nitrosyls are thus formed upon NO adsorption on the hydrated complexes, likely according to the following reaction:

$$Pd^{(II)}(OH)_2(H_2O)_2 + NO \rightarrow Pd^{(II)}(OH)_2(NO)(H_2O) + H_2O \quad (2)$$

Based on our FT-IR measurements, it is likely that reaction (2) may involve both $Pd^{(I)}$ and $Pd^{(II)}$ cations. $Pd^{(I)}$ cations may be obtained upon the reduction of $Pd^{(II)}$ by NO forming NO_2 [3636], although no NO_2 has been observed during our experiments.

Finally, the presence of nitrates-like species has also been observed in our experiments. As reported elsewhere [33,36], these species may be formed upon a weak interaction of NO with cation defect sites to form more thermally stable nitrate species (NO_3^-).

Notably, in the presence of water, FT-IR data have shown the absence of bands related to NO^+ species. This is explained by Chen et al. [6] who reported that H_2O could strongly interact with Brønsted acid sites making them inaccessible for NO.

After NO_x adsorption, the thermal stability of the stored NO_x has been analyzed by TPD. Gas-phase data are shown in Figure 7A, while the corresponding FT-IR spectra are in Figure 9A (temperature range 80-225°C) and 9B (temperature range 225-500°C). During the initial heating of the catalyst (Figure 9A), the bands at 1762 and 1812 cm^{-1} associated to hydrated Pd^{n+} nitrosyls decrease while, simultaneously, the band at 1866 with shoulder at 1844 cm^{-1} related to anhydrous Pd^{n+} nitrosyls increases. This clearly indicates that the stored hydrated palladium nitrosyls undergo decomposition and dehydration resulting in the evolution of NO (the low-T peak observe in Figure 7A) and in the formation of anhydrous nitrosyls (bands at 1866 cm^{-1} and shoulder at 1844 cm^{-1}). The formation of anhydrous nitrosyls from the corresponding hydrated ones is confirmed by the isosbestic point visible in the spectra of Figure 9A.

In the same temperature range, bands related to monodentate nitrates (in the region 1500-1300 cm^{-1}) rapidly decrease upon heating and they are almost completely removed below 150°C. These species may be decomposed and/or transformed into bidentate nitrate species whose presence is observed

upon catalyst dehydration. In fact, the band at 1618 cm^{-1}, assigned to adsorbed water, decreases upon heating, in line with the surface dehydration. This band becomes more symmetric and shifts towards higher wavenumbers, possibly indicating the presence of surface bidentate nitrates species (band at 1624 cm^{-1}), still present at 225°C. The transformation of bidentate nitrate species into monodentate/ionic moieties has been observed by some of us in a previous work [37] where we have demonstrated that water transforms bidentate species into monodentate/ionic ones. Therefore, it is suggested that the dehydration occurring during TPD leads to the transformation of monodentate nitrates into bidentate species and/or to their decomposition.

The complexes phenomena occurring at the surface during the initial part of the heating ramp (below 225°C), i.e. Pd-nitrosyls and nitrates decomposition/transformation, lead to the NO evolution that is observed with maxima at 100 and 160°C in the TPD trace (Figure 7A).

Upon further increasing the temperature in the range 225-500°C (Figure 9B), the bands related to Pd^{n+} nitrosyls (1866 and 1844 cm^{-1}) start to decrease and eventually disappear, indicating their thermal decomposition. The band of bidentate nitrates (1624 cm^{-1}) decreases as well and is completely consumed in the same temperature range.

The decomposition of these species results in a broad NO desorption peak with maximum at 370°C, already described in the gas phase analysis (Figure 7A), and leads to the complete regeneration of the surface at ca. 425°C.

3.3 Effect of CO during NO/O_2 adsorption

The effect of CO presence on NO_x adsorption has been investigated as well. Accordingly, the storage of NO/O_2 has been carried out in the presence of CO (800 ppm), and results are shown in Figure 10 (gas-phase analysis) and 11 (surface phase).

After the CO admission to the reactor (phase 1 in Figure 10), its concentration reaches rapidly the inlet value, showing a small adsorption. The FT-IR spectra recorded during the same phase (Figure 11A) have been interpreted on the basis of the results obtained by CO adsorption under static and

clean conditions at r.t. (Figure 3). Accordingly, bands at 2131 and 2115 cm^{-1} have been associated to Pd^{+} carbonyls, while bands related to Pd^{2+} are absent. Very likely, the presence of water inhibits the adsorption of CO on Pd^{2+}. Moreover, differently from the experiments under static conditions, in this case bands at 1967 and 1895 cm^{-1} assigned to bridged carbonyls of Pd^{+}/Pd^{0} and multi-bridged carbonyls on small clusters like Pd_3^{0} and Pd_3O, respectively, show higher relative intensities with respect to the linear carbonyl ones. Water adsorption is also observed, as pointed out by the increase of the band at 1620 cm^{-1}.

Under CO flow, NO is admitted to the reactor at 80°C (phase 2 of Figure 10). Upon NO admission, NO uptake is observed, with a simultaneous release of CO. This points out that NO displaces CO from the same storage sites. Then, the NO concentration reaches a steady level; no NO_2 evolution is observed during the NO storage. The results of FT-IR surface analysis upon NO admission in the presence of CO are shown in Figure 11B, that refers to phase 2 of Figure 10. NO admission leads to the formation of Pd-nitrosyls species (bands in the region 1850-1750 cm^{-1}) while a concomitant erosion of the bands of Pd carbonyl in the region 2140-1890 cm^{-1} is observed. This clearly confirms the CO displacement by NO, although small bands related to the presence of CO are still present after NO admission (very weak band at 2131 cm^{-1} and 1965 cm^{-1}). It is worth of note that Pd^{2+} nitrosyls are also formed, while CO is not able to adsorb on Pd^{2+} in the presence of water and CO_2 in the feed. This result points out the different bonding strength of CO and NO with Pd^{2+}, being NO able to displace water and to form hydrated nitrosyls according to reaction (2). Notably, any evidence of mixed Pd(II)(CO)(NO) complex formation has been found in the course of our experiments. Besides, no nitrate bands in the region 1500-1300 cm^{-1} are observed.

The amounts of stored NO_x in this case is near 40 $\mu mol/g_{cat}$, corresponding to a NO / Pd molar ratio of 0.4. This value is lower than that measured in the absence of CO, thus indicating that CO has a negative impact on NO adsorption, as discussed below.

At the end of phase 2, the NO is switched off and the heating ramp starts (phase 3 in Figure 10). Initially, no NO_x desorption is observed but near 120°C a very sharp NO peak is observed, with a tail

that extends up to 300°C. The sharp NO desorption peak is accompanied by a very fast consumption of CO, leading to CO_2 production in the gas phase. The FT-IR spectra recorded during this phase (Figure 11C) show an initial transformation of the nitrosyls (decrease of the band at 1764 cm^{-1} and increase of the band at 1864 cm^{-1}), like in the absence of CO. Then, in the range 125-175°C, an abrupt decrease of the Pd-nitrosyl bands is observed, accompanied by a sharp NO peak observed in the gas phase (Figure 10). The formation of gaseous CO_2 (roto-vibrational feature at about 2341 cm^{-1}) is also observed, in well agreement with the CO oxidation to CO_2 observed in the gas phase.

These particular features may be explained by considering that upon increasing the temperature, starting from ~100°C, CO becomes effective in the reduction of Pd sites, being CO oxidized to CO_2. Accordingly, formation of carbonyls is no more observed during the experiment. The reduction of the Pd sites leads to the fast decomposition of the nitrosyls, leading to NO desorption, being reduced Pd ineffective in the NO storage. This process may also be favored by the exothermicity of the CO oxidation reaction that leads to an increase of the temperature of the Pd storage sites.

As reported above, when the NO adsorption is carried out in the presence of CO, a significant decrease in the amounts of stored NOx is observed (40 vs. 59 $\mu mol/g_{cat}$). At variance, in recent studies it has been shown that the presence of CO in the feed promotes the NO_x uptake, mitigating the inhibition of water [8,38]. In particular, it has been claimed that stable mixed Pd(II) carbonyl nitrosyl complex are formed, responsible for the observed enhanced NO_x storage [33,38]. Our study clearly shows that NO displaces CO from Pd sites, but no positive effect has been observed. Besides, nitrate formation has also been reduced in the presence of CO. The same effect has also been observed over a Pd/CHA sample [to be published], and therefore is not related to the FER sample used in this study. These differences might be related to the different operating conditions used in this study (sequential feed of CO and then of NO, slightly different temperature, absence of NO during the heating ramp) and investigations are presently ongoing to address this point.

4. Conclusions

In this study a Pd-promoted FER zeolite has been synthesized and investigated for potential use in the low-temperature NO_x adsorption. It has been shown that calcination temperature affects the catalytic performances, in that the sample calcined at high temperature (750 °C) presents better NO_x adsorption capacity, very likely due to the higher Pd dispersion. TEM analysis carried out over the oxidized sample showed that Pd is present as PdO_x clusters/particles; roughly 13% of Pd is also in the form of isolated Pd^{n+} ions, as detected by NaCl titration.

Pd species have also been probed by NO and CO adsorption experiments, that showed the existence of nitrosyl and carbonyl species, respectively, over Pd^{+} and Pd^{2+} cations, with different dispersion (both isolated moieties and small particles). CO adsorption also showed the presence of extraframework Al^{3+} while NO^{+} species have been observed in the case of NO adsorption in the absence of water.

Acid sites have been probed by NH_3 adsorption and NaCl exchange; near 0.3 mmol/g_{cat} of Bronsted acid sites have been estimated with NH_3 in the case of the bare FER sample. This value is lower than that expected from the Al content in the zeolite, possibly due to the presence of extraframework Al. Addition of Pd to FER leads to a reduction of the Bronsted acid sites, due the exchange of surface protons with Pd leading to the formation of isolated Pd ions.

Catalyst reduction leads to an almost complete loss of CO adsorption capacity, likely due to formation of big reduced Pd particles. Re-oxidation restores the adsorption Pd^{n+} sites, with a marked increase of the Pd^{2+} species at the expense of Pd^{+}.

The NO_x storage capacity of Pd_1/FER has been evaluated at 80°C in the presence of CO_2 and H_2O. The Pd_1/FER sample calcined at 750°C shows significant NO_x adsorption capacity, near 59 µmol/g_{cat}, corresponding to a NO / Pd molar ratio near 0.6. *Operando* FT-IR spectroscopy pointed out the formation of Pd^{2+} and Pd^{+} nitrosyls during NO/O_2 adsorption, both in the hydrated and anhydrous form; bands related to monodentate nitrates are also apparent.

Upon heating, the stored NO_x desorb exclusively as NO. Two major contributions are observed, namely a low-temperature peak below 200°C and a high temperature peak above 300°C. The low

temperature NO desorption peak is associated to the decomposition of monodentate nitrates and of a part of the hydrated Pd^{n+} nitrosyls; these species also undergo dehydration to anhydrous nitrosyls in the same T range. The high temperature NO peak (with maximum at 370°C) is on the other hand associated to the decomposition of the anhydrous Pd^{n+} nitrosyls and of bidentate nitrates.

The presence of CO affects both the amounts and the stability of the stored NO_x. Pd^+ carbonyls are formed in the presence of CO, along with bridged carbonyls of Pd^+/Pd^0 and multi-bridged carbonyls on small clusters like Pd_3^0 and Pd_3O, respectively. NO displaces Pd carbonyls leading to the formation of Pd nitrosyls; however the NO_x storage capacity is reduced in the presence of gas-phase CO, from 59 down to 40 $\mu mol_{NO}/g_{cat}$.

The stability of the stored nitrosyls is also modified by the presence of CO, being NO released at lower temperature and with a sharp peak.

Lidia Castoldi: Conceptualization, writing original draft
Roberto Matarrese: investigation, methodology
Sara Morandi: investigation, writing original draft
Pierfrancesco Ticali: investigation
Luca Lietti: supervision, writing review & editing, funding acquisition

Declaration of interests

The authors declare that they have no known competing financial interests or personal relationships that could have appeared to influence the work reported in this paper.

Aknowledgement

LL and RM gratefully acknowledge the contribution of Fondazione Banca del Monte di Lombardia for the FTIR-operando set-up

References

[1] A. Walker, Top. Catal. 59 (2016) 695-707.

[2] Y. Ji, S. Bai, M. Crocker, Appl. Catal. B Environ. 170–171 (2015) 283-292.

[3] J.R. Theis, C.K. Lambert, Catal. Today 258 (2015) 367-377.

[4] S. Tamm, S. Andonova , L. Olsson, Catal. Lett. 144 (2014) 674-684.

[5] S. Jones, Y. Ji, M. Crocker, Catal. Lett. 146 (2016) 909-917.

[6] H-Y Chen, J. E. Collier, D. Liu, L. Mantarosie, D. Durán-Martín, V. Novák, R.R. Rajaram, D. Thompsett, Catal Letters 146 (2016) 1706-1711.

[7] Y. Murata, T. Morita, K. Wada, H Ohno, SAE Int. J. Fuels Lubr. 8 (2015):1–6

[8] Y. Zheng, L. Kovarik, M.H. Engelhard, Y. Wang, Y. Wang, F. Gao, J. Szanyi, J Phys Chem C 121 (2017) 15793-15803.

[9] Y.S. Ryou, J. Lee, H. Lee, C. Kim, C. Kim, Catal. Today 307 (2018) 93-101.

[10] J. Lee, Y.S. Ryou, S.J. Cho, H. Lee, C. H. Kim, D. H. Kim, Appl. Catal. B Environ. 226 (2018) 71-82.

[11] A. Porta, T. Pellegrinelli, L. Castoldi, R. Matarrese, S. Morandi, S. Dzwigaj, L. Lietti, Top. Catal. 61 (2018) 2021-2034.

[12] J.E. Schmidt, F.C. Hendriks, M. Lutz, L.C. Post, D. Fu, B.M. Weckhuysen, Chem. Phys. Chem. 19 (2018) 367-372.

[13] A. Gervasini, Appl. Catal. A: General 180 (1999) 71-82.

[14] J.H. de Boer, B.G. Linsen, T.J. Osinga, J. Catal. 4 (1964) 643.

[15] Collection of Simulated XRD Powder Patterns for Zeolites, Editors M.M.J. Treacy and J.B. Higgins, Fourth Revised Edition ELSEVIER, 2001

[16] K.I. Hadjiivanov, G.N. Vayssilov, Adv. Catal. 47 (2002) 307-511.

[17] A.W. Aylor, L.J. Lobree, J.A. Reimer, A.T. Bell, J. Catal. 172 (1997) 453-462

[18] K. Chakarova, E. Ivanova, K. Hadjiivanov, D. Klissurski, H. Knözinger, Phys. Chem. Chem. Phys. 6 (2004) 3702-3709.

[19] K. Khivantsev, N.R. Jaegers, I.Z. Koleva, H.A. Aleksandrov, L. Kovarik, M. Engelhard, F. Gao, Y. Wang, G.N. Vayssilov , J. Szanyi, (2019): Stabilization of Super Electrophilic Pd+2 Cations in Small-Pore SSZ-13 Zeolite, ChemRxiv, Preprint.

[20] G. Spezzati, Y. Su, J. P. Hofmann, A. D. Benavidez, Andrew T. DeLaRiva, J. McCabe, A. K. Datye, E. J. M. Hensen, ACS Catal. 7 (2017) 6887−6891.

[21] K. Khivantsev, N. R. Jaegers, L. Kovarik, J. C. Hanson, F. Tao, Y. Tang, X. Zhang, I. Z. Koleva, H. A. Aleksandrov, G. N. Vayssilov, Y. Wang, F. Gao, J. Szanyi, Angew. Chem. Int. Ed. 57 (2018) 16672–16677.

[22] B. Onida, F. Geobaldo, F. Testa, F. Crea, E. Garrone, Micropor. Mesopor. Mat. 30 (1999) 119–127.

[23] Y.S. Ryou, J. Lee, Y. Kim, S. Hwang, H. Lee, C. H. Kim, D. H. Kim, Appl. Catal. A General 569 (2019) 28-34.

[24] A. Zecchina, L. Marchese, S. Bordiga, C. Paze and E. Gianotti, J. Phys. Chem. B 101 (1997) 10128

[25] Bortnovsky, O.; Melichar, Z.; Sobalik, Z.; Wichterlova, B. Microporous Mesoporous Mater. 2001, 42, 97

[26] I. Lezcano-Gonzales, U. Deka, B. Arstad, A. Van Yperen-De Deyna, K. Hemelsoet, M. Waroquier, V. Van Speybroeck, B. M. Weckhuysen, A. M. Beale, Phys. Chem. Chem. Phys. 16 (2014) 1639.

[27] K.I. Hadjivanov Catal. Rev.- Sci. Eng. 42 (2000), 71–144.

[28] C. Descorme, P. Gélin, C. Lécuyer, M. Primet, J. Catal 177 (1998) 352-362.

[29] K. Khivantsev, N. R. Jaegers, L. Kovarik, S. Prodinger, M.A. Derewinski, Y. Wang, F. Gao, J. Szanyi, Appl. Cat. A: General 569 (2019) 141-148

[30] K.I. Hadjiivanov, J. Saussey, J.L. Freysz, J.C. Lavalley, Catal. Lett. 52 (1998) 103–108

[31] Y.S. Ryou, J. Lee, H. Lee, C.H. Kim, D.H. Kim, Catal. Today 320 (2019) 175–180.

[32] L.J. Lobree, A.W. Aylor, A.J. Reimer, A.T. Bell, J. Catal. 181 (1999) 189.

[33] C. Descorme, P. Gélin, M. Primet, C. Lécuyer, Catal. Lett. 41 (1996) 133-138.

[34] M. Boronat, A. Corma, ACS Catal., 9 (2019) 1539−1548.

[35] Y. Gu, W.S. Epling, Appl. Catal. A General 570 (2019) 1-14

[36] C. Sedlmair, B. Gil, K. Seshan, A. Jentys, J.A. Lercher, Phys. Chem. Chem. Phys. 5 (2003) 1897–1905.

[37] S. Morandi, F. Prinetto, L. Castoldi, L. Lietti, P. Forzatti, G. Ghiotti, Phys. Chem. Chem. Phys. 15 (2013) 13409–13417.

[38] K. Khivantsev, F. Gao, L. Kovarik, Y. Wang, J. Szanyi, J. Phys. Chem. C 122 (2018) 10820-10827.

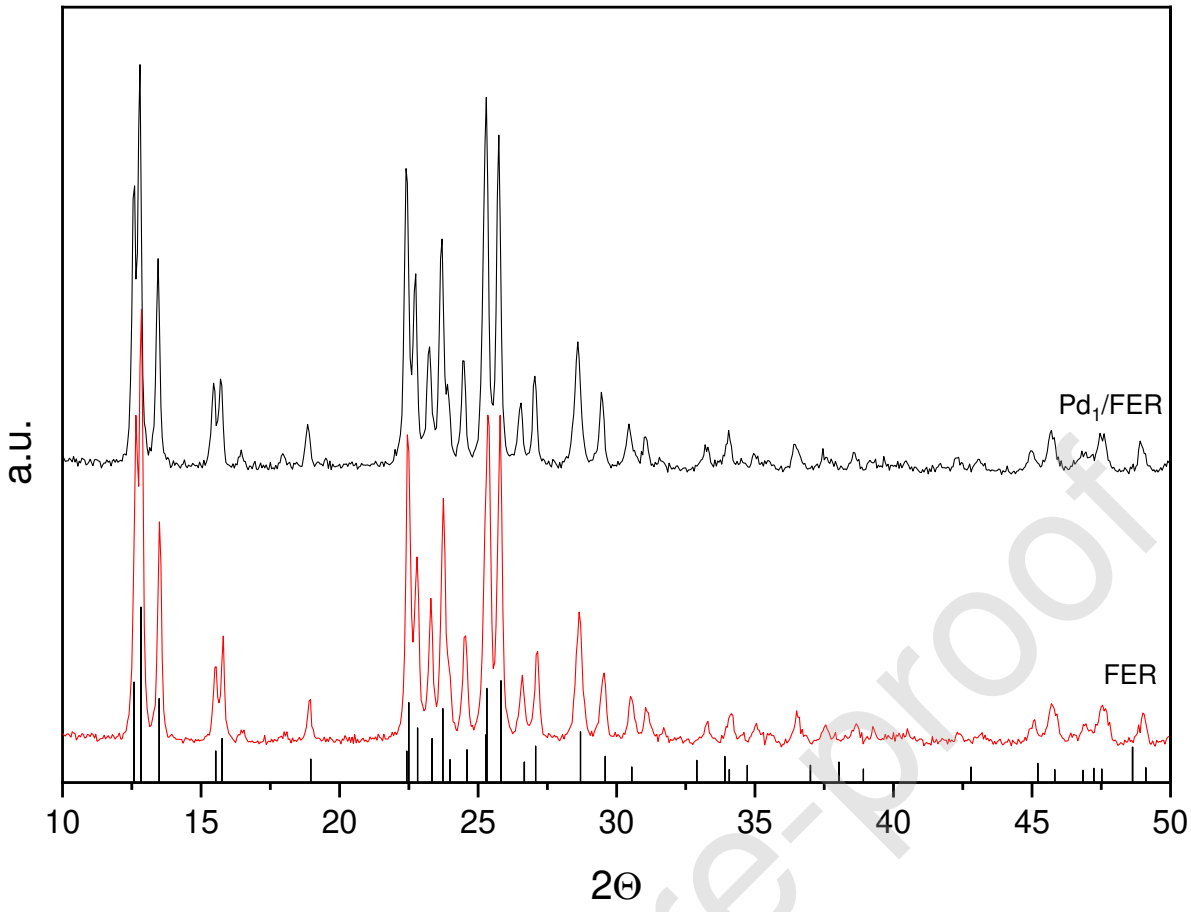

Figure 1 – X-ray diffraction (XRD) spectra of bare FER and Pd_1/FER zeolite. The reference pattern of FER framework is also reported

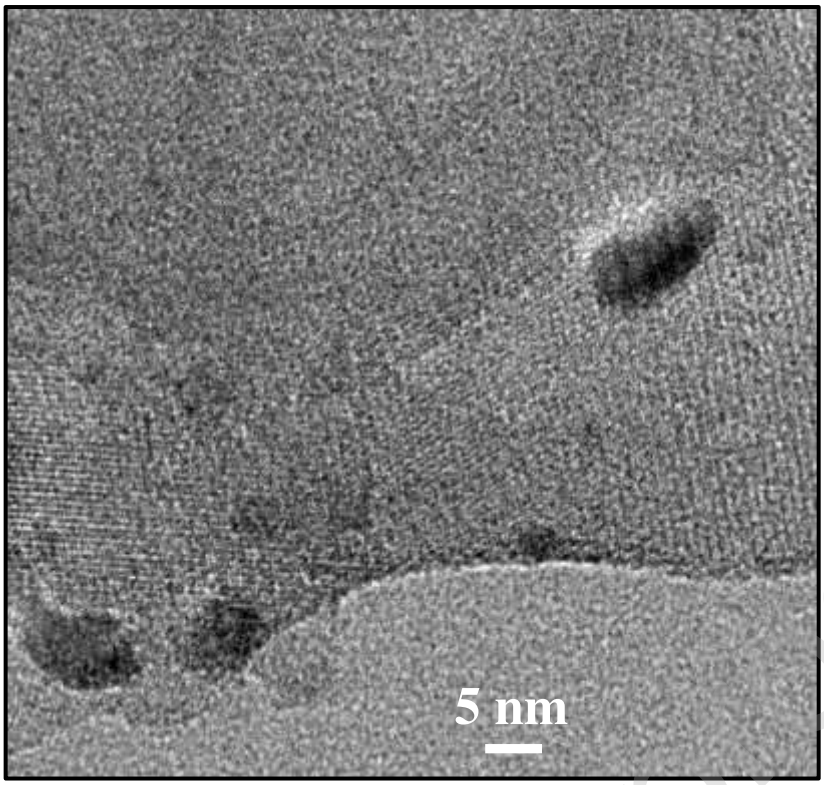

Figure 2 – TEM image of Pd_1/FER after oxidation at 500°C with 40 mbar of O_2.

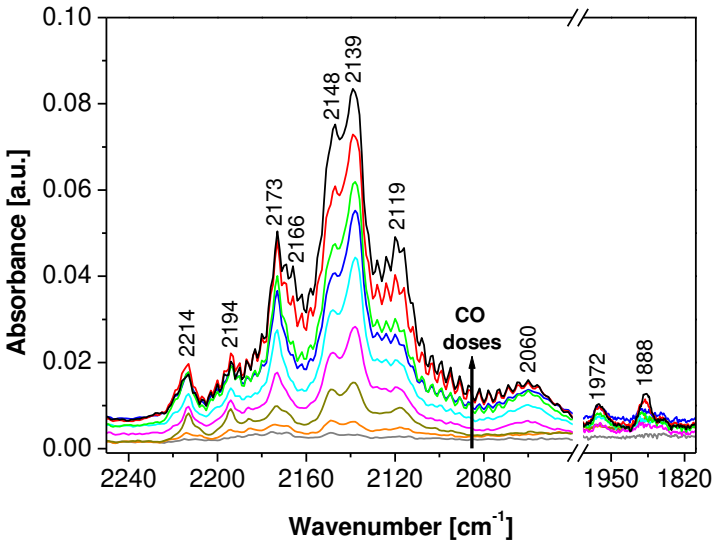

Figure 3 – FT-IR spectra of CO adsorption at increasing pressure up to 20 mbar and at r.t. on a pre-oxidized Pd_1/FER catalyst. Experimental conditions: O_2 (40 mbar) at 500°C

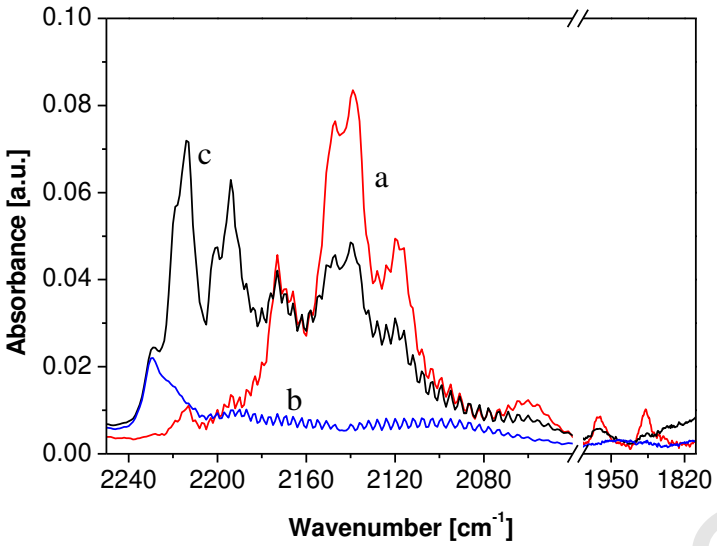

Figure 4 – FT-IR spectra of CO adsorption (20 mbar) at r.t. on Pd_1/FER after different pretreatment: oxidation at 500°C in 40 mbar of O_2 (a curve); reduction at 500°C in 40 mbar of H_2 (b curve); re-oxidation at 500°C in 40 mbar of O_2 (c curve)

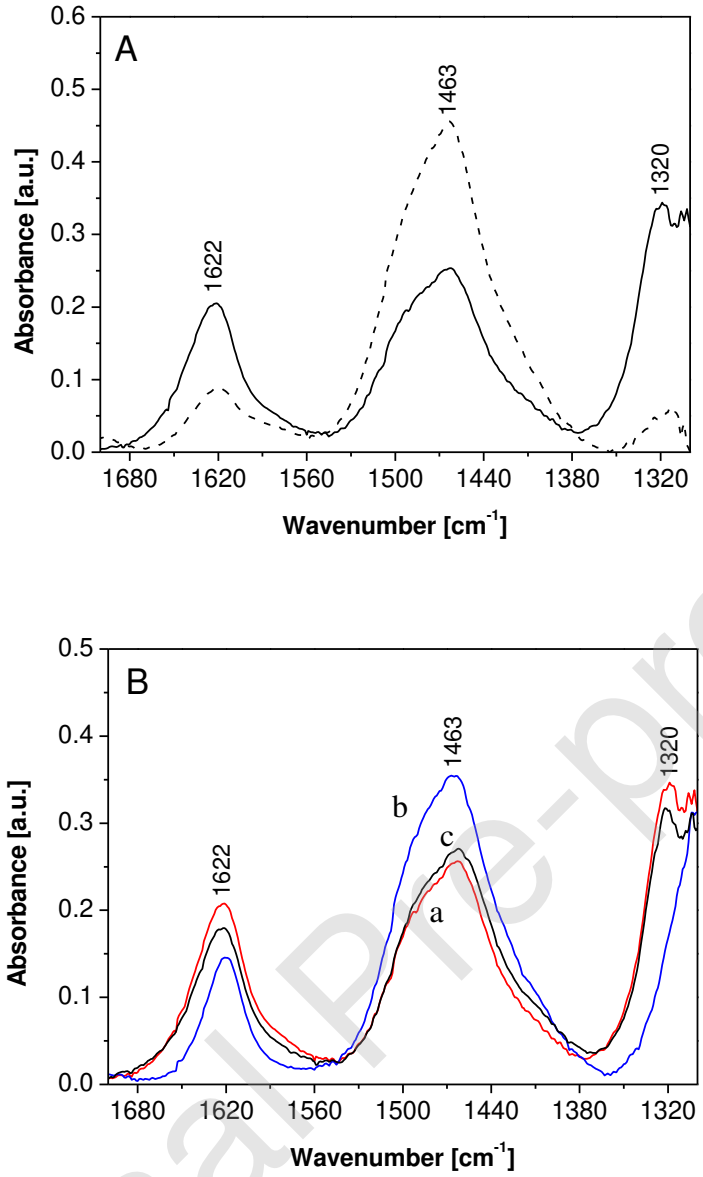

Figure 5 – FT-IR spectra after NH_3 adsorption and subsequent evacuation at r.t. on A) FER (dashed curve) and Pd_1/FER (solid curve) both oxidized at 500 °C in 40 mbar of O_2; B) Pd_1/FER after different pretreatment: oxidation at 500°C in 40 mbar of O_2 (a curve); reduction at 500°C in 40 mbar of H_2 (b curve); re-oxidation at 500°C in 40 mbar of O_2 (c curve).

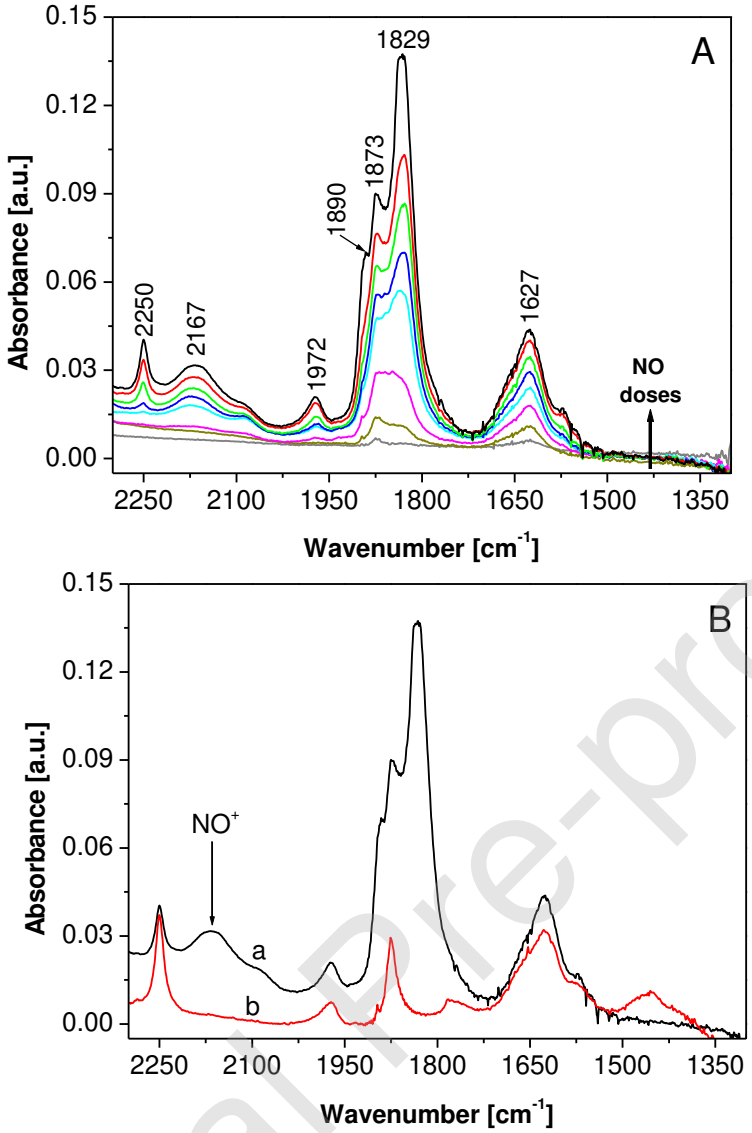

Figure 6 – Section A: FT-IR spectra on Pd_1/FER pre-treated in O_2 at 500°C: NO adsorption at increasing pressure up to 2 mbar at r.t.. Section B: comparison between the FT-IR spectra obtained after adsorption of 2 mbar of NO on Pd_1/FER pre-treated in O_2 at 500°C (a curve) and pre-treated in H_2 at 500°C (b curve).

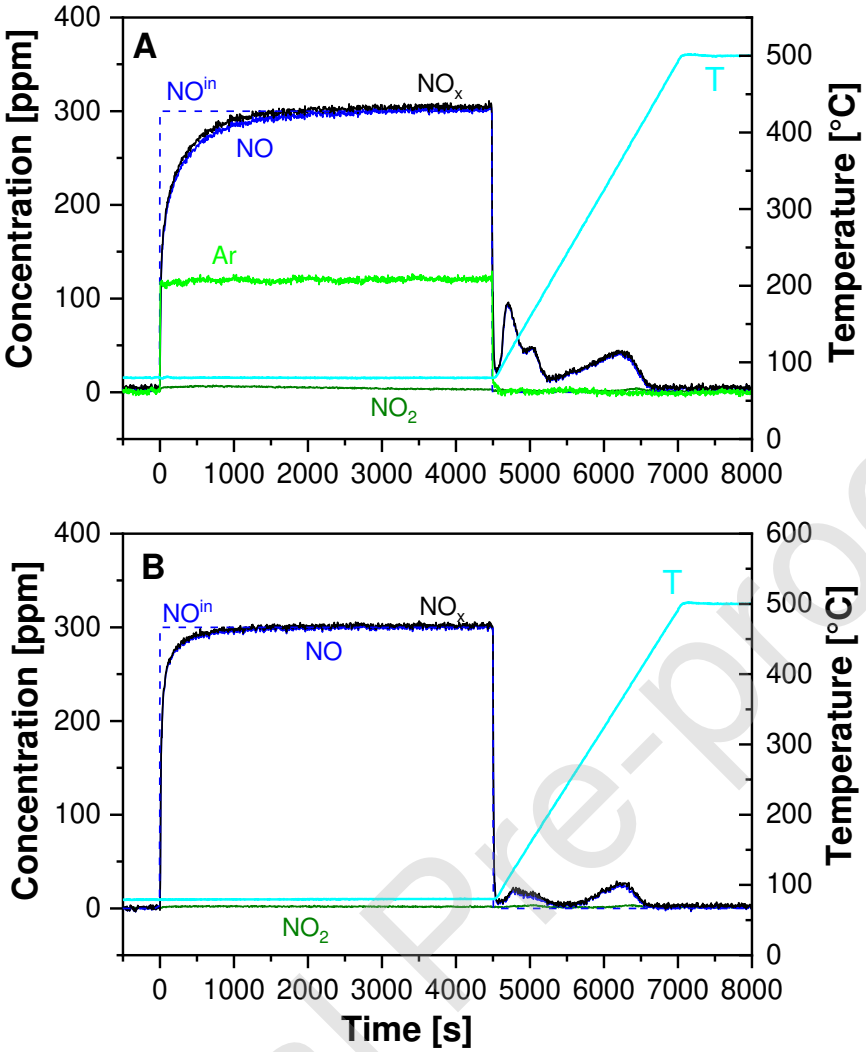

Figure 7 – NO/O_2 adsorption at 80°C and subsequent TPD experiment over A) Pd_1/zeolite calcined at 750°C; B) Pd_1/FER calcined at 500°C. Experimental conditions: storage phase NO (300 ppm) + O_2 (3%) + CO_2 (2%) + H_2O (2,5%) in He; TPD in O_2 (3%) + CO_2 (2%) + H_2O (2,5%) in He from 80°C to 500°C (10°/min).

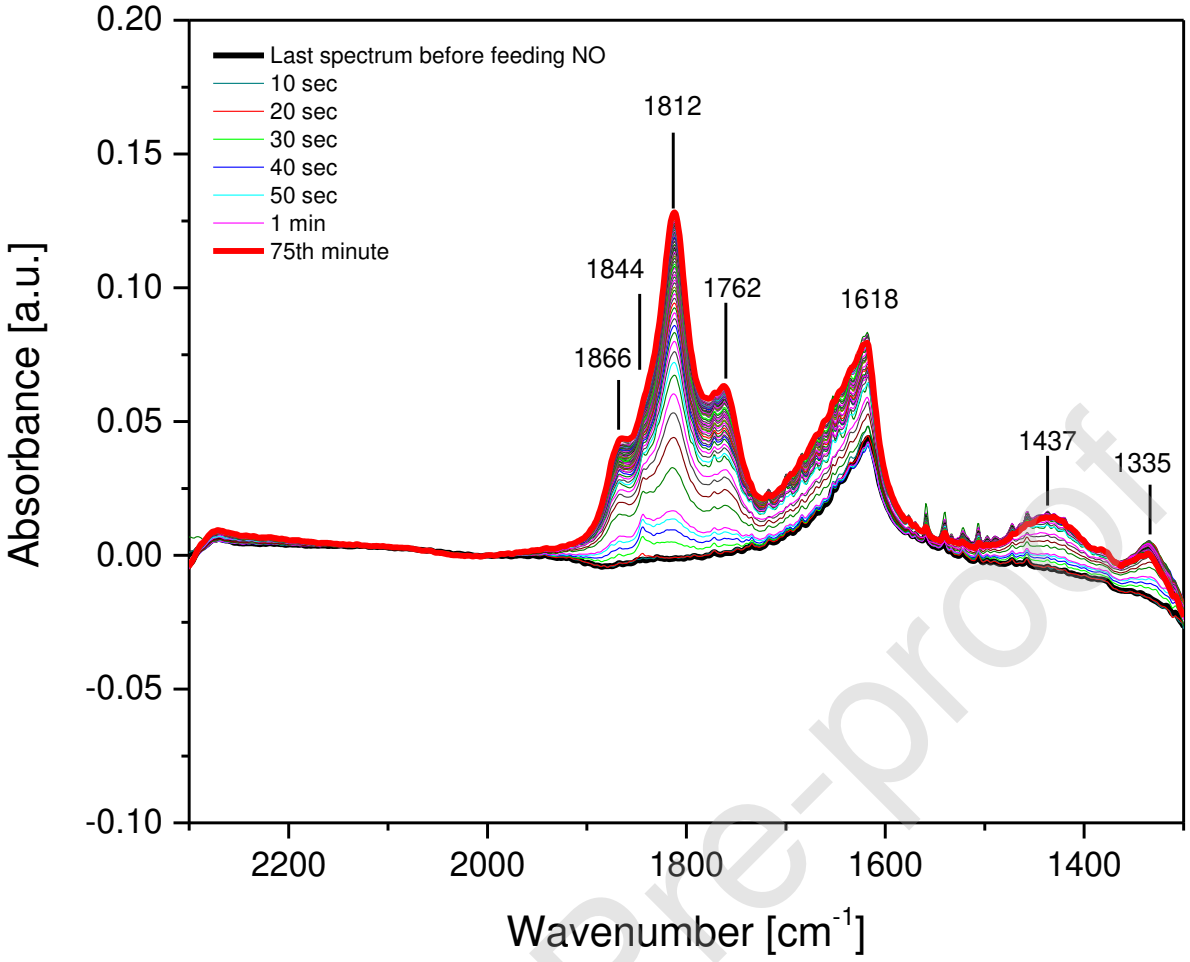

Figure 8 – FT-IR spectra collected during the NO/O_2 adsorption at 80°C over Pd_1/FER calcined at 750°C. Experimental conditions: storage phase NO (300 ppm) + O_2 (3%) + CO_2 (2%) + H_2O (2,5%) in He.

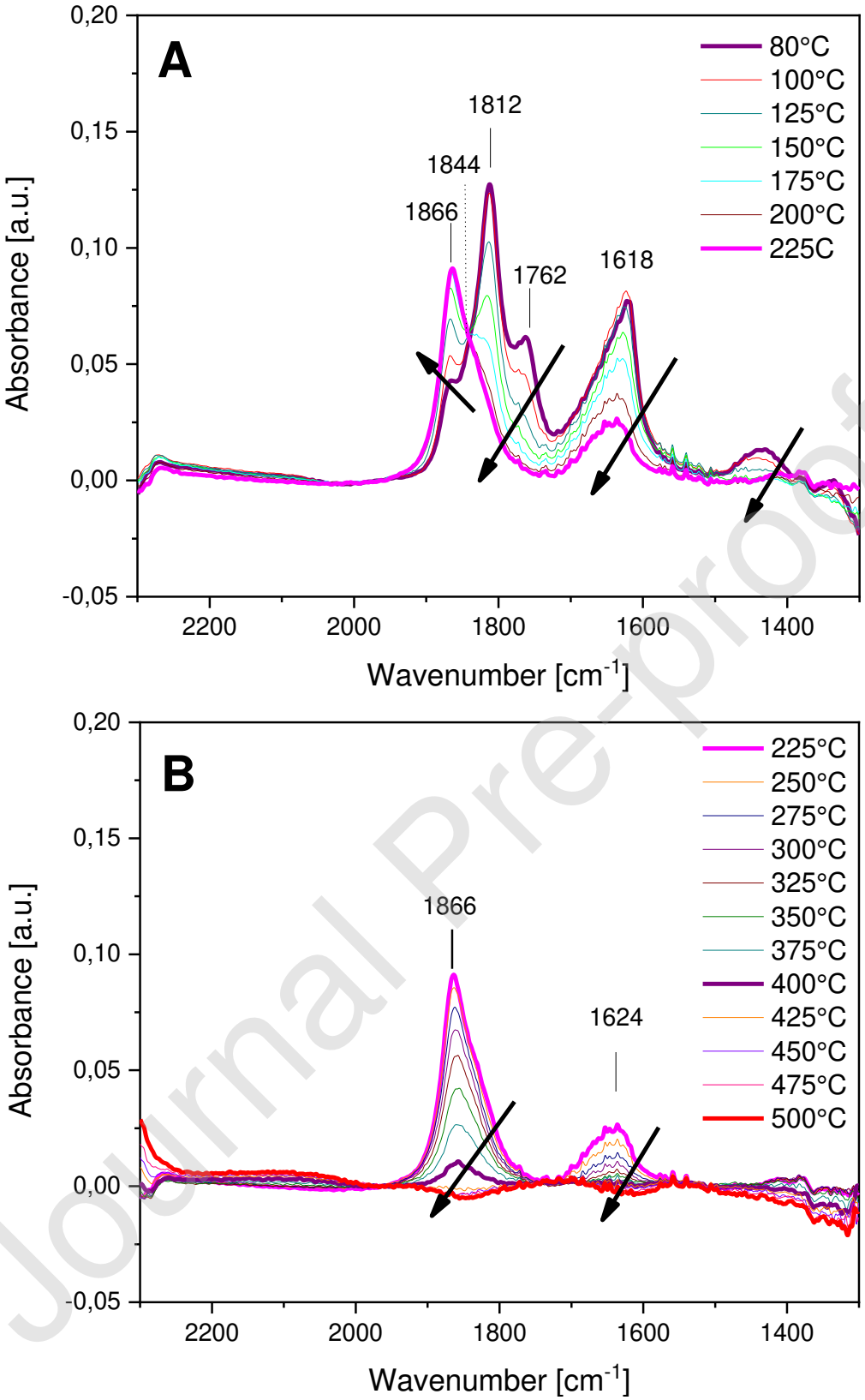

Figure 9 – FT-IR spectra collected during Temperature Programmed Desorption (TPD) after NO adsorption at 80°C (Figure 8).

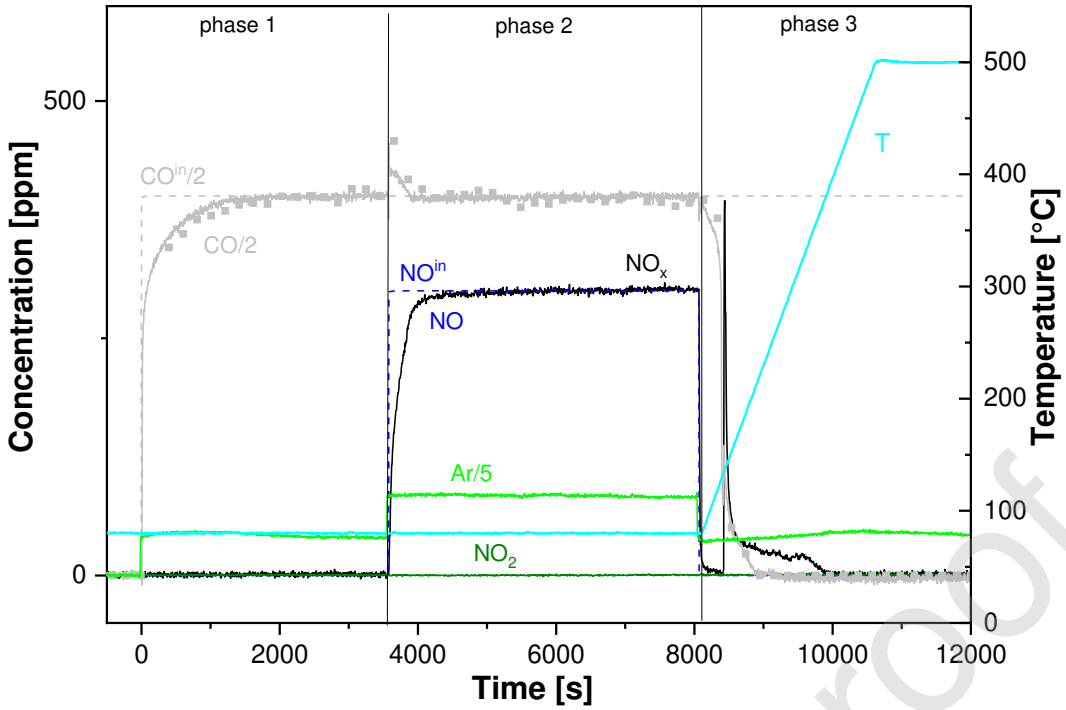

Figure 10 – NO/O_2 adsorption at 80°C in the presence of CO and subsequent TPD experiment over Pd_1/FER. Experimental conditions: storage phase NO (300 ppm) + CO (800 ppm) + O_2 (3%) + CO_2 (2%) + H_2O (2,5%) in He; TPD in O_2 (3%) + CO_2 (2%) + H_2O (2,5%) + CO (800 ppm) in He from 80°C to 500°C (10°/min)

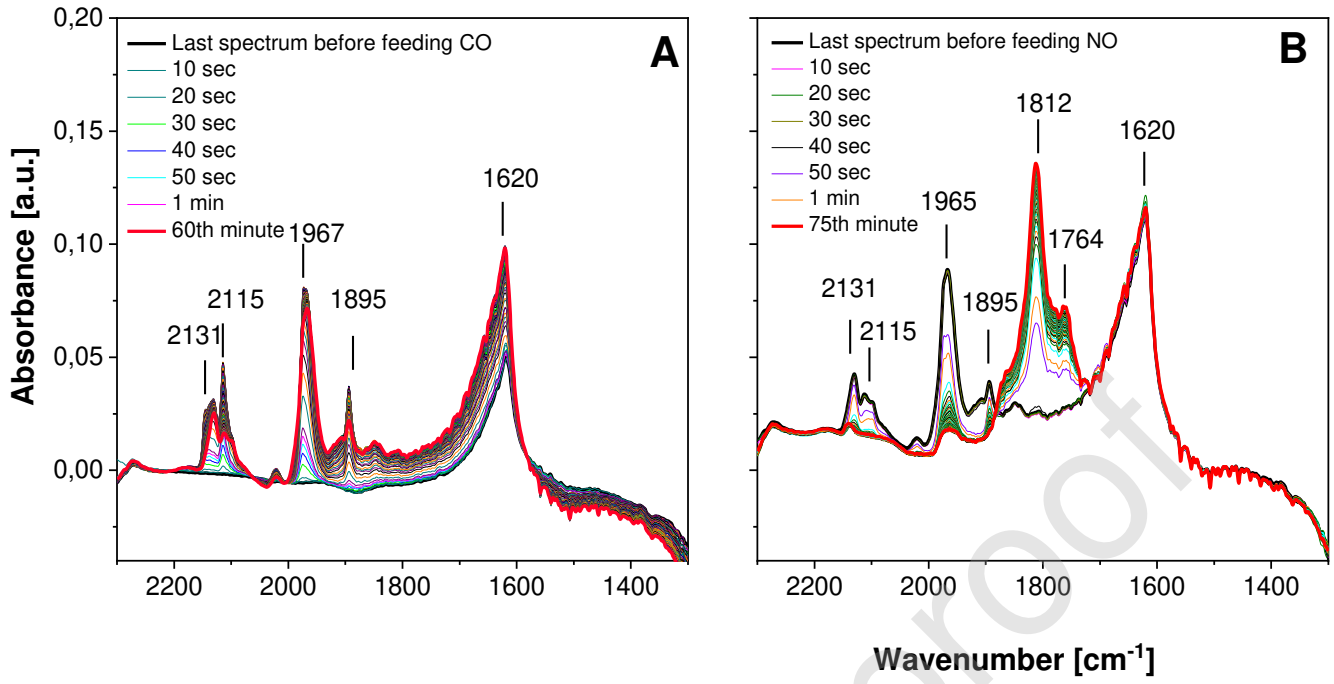

Figure 11 – FT-IR spectra collected during spectra collected during NO/O_2/CO adsorption at 80°C and subsequent TPD experiment Pd_1/FER. A) adsorption of CO referring to phase 1 in Figure 10; B) adsorption of NO/O_2 referring to phase 2 in Figure 10; C-D) TPD referring to phase 3 in Figure 10. Experimental conditions: storage phase CO (800 ppm) + O_2 (3%) + CO_2 (2%) + H_2O (2,5%) in He at 80°C. TPD in O_2 (3%) + CO_2 (2%) + H_2O (2,5%) + CO (800 ppm) in He from 80°C to 500°C (10°/min)